J|A|C|S ARTICLES

Published on Web 12/19/2008

Reorganization Energies of Diprotonated and Saddle-Distorted Porphyrins in Photoinduced Electron-Transfer Reduction Controlled by Conformational Distortion

Tatsuaki Nakanishi, Kei Ohkubo, Takahiko Kojima,* and Shunichi Fukuzumi*

Department of Material and Life Science, Graduate School of Engineering, Osaka University and SORST (JST), 2-1 Yamada-oka, Suita, Osaka 565-0871, Japan

Received August 8, 2008; E-mail: kojima@chem.eng.osaka-u.ac.jp; fukuzumi@chem.eng.osaka-u.ac.jp

Abstract: Kinetics of photoinduced electron transfer from a series of electron donors to the triplet excited states of a series of nonplanar porphyrins, hydrochloride salts of saddle-distorted dodecaphenylporphyrin ($[H_4DPP]Cl_2$), tetrakis(2,4,6-trimethylphyenyl)porphyrin ($[H_4TMP]Cl_2$), tetraphenylporphyrin ($[H_4TPP]Cl_2$), and octaphenylporphyrin ($[H_4OPP]Cl_2$), were investigated in comparison with those of a planar porphyrin, zinc [tetrakis(pentafluorophenyl)]porphyrin [$Zn(F_{20}TPP)(CH_3CN)$], in deaerated acetonitrile by laser flash photolysis. The resulting data were evaluated in light of the Marcus theory of electron transfer, allowing us to determine reorganization energies of electron transfer to be 1.21 eV for $[H_4TMP]Cl_2$, 1.29 eV for $[H_4TPP]Cl_2$, 1.45 eV for $[H_4OPP]Cl_2$, 1.69 eV for $[H_4DPP]Cl_2$, and 0.84 eV for $[Zn(F_{20}TPP)(CH_3CN)]$. The reorganization energies exhibited a linear correlation relative to the out-of-plane displacements, which represent the degree of nonplanarity. The rate of electron-transfer reduction of diprotonated porphyrins is significantly slowed down by conformational distortions of the porphyrin ring. This indicates that the reorganization energy of electron transfer is governed by structural change, giving a larger contribution of inner-sphere bond reorganization energy rather than outer-sphere solvent reorganization energy.

Introduction

Porphyrins contain an extensively conjugated π system, which enables efficient electron transfer, because the uptake or release of electrons from porphyrins usually results in minimal structural change upon electron transfer.[1] The redox properties of porphyrins are significantly altered by light absorption forming the singlet excited states that are converted by intersystem crossing to the triplet excited states, which have long lifetimes.[2] Such extremely rich redox properties of the ground and excited states render porphyrins essential components in important biological electron-transport systems including photosynthesis and respiration.[2−9] Thus, the electron-transfer properties of porphyrins have been receiving great attention.[10−12] According to the Marcus theory of electron transfer,[13] the reorganization energy (λ) of electron transfer is the energy required to structurally reorganize the donor, acceptor, and their solvation spheres upon electron transfer and the λ value is an important factor to determine the electron-transfer reactivity. Despite the important roles of porphyrins in a variety of electron-transfer reactions in chemical and biological systems, surprisingly little is known about the reorganization energies of porphyrins, in particular for macrocycle-centered electron-transfer reactions.[1,14]

Although porphyrins normally have a planar π plane, nonplanar conformations of porphyrins have been suggested as being related to their functions in biological systems.[15,16] For example, a deformation of the porphyrin skeleton in heme and photosynthetic proteins has been believed to arise from environmental effects.[16−18] Synthetic dodecaphenylporphyrin (H_2DPP), which contains a phenyl ring at each β-pyrrole and

(1) Fukuzumi, S. In *The Porphyrin Handbook*; Kadish, K. M., Smith, K., Guilard, R., Eds.; Academic Press: San Diego, CA; 2000; Vol. 8, p 115.
(2) (a) Deisenhofer, J.; Michel, H. *Angew. Chem., Int. Ed. Engl.* **1989**, *28*, 829. (b) von Jagow, G.; Engel, W. D. *Angew. Chem., Int. Ed. Engl.* **1980**, *19*, 659.
(3) Dickerson, R. E.; Timkovich, R. *The Enzymes*, 3rd ed.; Boyer, P., Ed.; Academic Press: New York, 1975; Vol. 11, p 397.
(4) Kaim, W.; Schwederski, B. *Bioinorganic Chemistry: Inorganic Elements in the Chemistry of Life*; Wiley: New York, 1994.
(5) Margoliash, E. In *Electron Transport and Oxygen Utilization*; Ho, C., Ed.; Elsevier: New York, 1982.
(6) Isied, S. S. *Prog. Inorg. Chem.* **1984**, *32*, 443.
(7) Meyer, T. E.; Kamen, M. D. *Adv. Protein Chem.* **1982**, *35*, 105.
(8) Sigel, H.; Sigel, A., Eds. *Electron Transfer Reactions in Metalloproteins, in Metal Ions in Biological Systems*; Marcel Dekker: New York, 1991; Vol. 27.
(9) Moore, G. R.; Pettigrew, G. W. *Cytochromes c*; Springer-Verlag: Berlin, 1990.
(10) Fukuzumi, S.; Imahori, H. In *Electron Transfer in Chemistry*; Balzani, V., Ed.; Wiley-VCH: Weinheim, 2001; Vol. 2, p 927.
(11) Kadish, K. M.; Van-Caemelbecke, E.; Royal, G. In *The Porphyrin Handbook*; Kadish, K. M., Smith, K. M., Guilard, R., Eds.; Academic Press: San Diego, 2000; Vol. 8, p 1.
(12) Gust, D.; Moore, T. A. In *The Porphyrin Handbook*; Kadish, K. M., Smith, K. M., Guilard, R., Eds.; Academic Press: New York, 2000; Vol. 8, p 153.
(13) (a) Marcus, R. A. *Annu. Rev. Phys. Chem.* **1964**, *15*, 155. (b) Marcus, R. A. *Angew. Chem., Int. Ed. Engl.* **1993**, *32*, 1111.
(14) For λ values for metal-centered electron-transfer reactions of metalloporphyrins, see:(a) Fukuzumi, S.; Nakanishi, I.; Tanaka, K.; Suenobu, T.; Tabard, A.; Guilard, R.; Van Caemelbecke, E.; Kadish, K. M. *J. Am. Chem. Soc.* **1999**, *121*, 785.
(15) (a) Horning, T. L.; Fujita, E.; Fajer, J. *J. Am. Chem. Soc.* **1986**, *108*, 323. (b) Barkigia, K. M.; Renner, M. W.; Genge, M. O.; Fajer, J. *J. Phys. Chem. B* **2004**, *108*, 2173. (c) Marcelli, A.; Foggi, P.; Moroni, L.; Gellini, C.; Salvi, P. R.; Badovinac, I. J. *J. Phys. Chem. A* **2007**, *111*, 2276. (d) Marcelli, A.; Foggi, P.; Moroni, L.; Gellini, C.; Salvi, P. R. *J. Phys. Chem. A* **2008**, *112*, 1864.

meso position of the porphyrin macrocycle, is known to adopt a nonplanar conformation.[1,19−21] The effects of porphyrin ring nonplanarity due to steric repulsion among ring substituents in dodecasubstituted porphyrins on their optical properties have also been reported.[19−23] The saddle-distorted structure of H_2DPP provides a curved surface, which has been self-assembled to construct a novel porphyrin nanochannel, composed of the doubly protonated porphyrin dications (H_4DPP^{2+}).[24,25] The doubly protonated porphyrin dications (H_4DPP^{2+}), which are readily obtained due to distortion, can act as an electron acceptor, whereas unprotonated porphyrins usually act as electron donors rather than acceptors.[10−12,26] There have been some studies on electron-transfer reduction of metalloporphyrins;[27−30] however, the site of electron transfer is not at the porphyrin ring but at the redox-active metal.[28−30] Thus, the electron-transfer properties of such doubly protonated porphyrins without metal ions acting as electron acceptors in thr electron-transfer reaction in solution have yet to be examined. In addition, there have been so far no reports on how conformational distortions of the porphyrin ring affect the rates of homogeneous electron-transfer reactions of diprotonated porphyrins.

We report herein the detailed photoinduced electron-transfer kinetics for the reduction of a series of nonplanar porphyrins, hydrochloride salts of saddle-distorted dodecaphenylporphyrin ($[H_4DPP]Cl_2$), tetrakis(2,4,6-trimethylphenyl)porphyrin ($[H_4TMP]Cl_2$), tetraphenylporphyrin ($[H_4TPP]Cl_2$), and octaphenylporphyrin ($[H_4OPP]Cl_2$), in comparison with that of a planar porphyrin, (acetonitrile-κN)(tetrakis(pentafluorophenyl)porphyrinato)zinc(II) ([Zn(F_{20}TPP)(MeCN)]), examined by laser flash photolysis. The resulting rate data are evaluated in light of the Marcus theory of electron tranfer[13] to determine reorganization energies of photoinduced electron transfer of diprotonated porphyrins with different degrees of distortion of the porphyrin ring. The present study provides valuable insight into how conformational distortions of the porphyrin ring affect the rates of intermolecular electron-transfer reduction of diprotonated porphyrins in solution.

Experimental Section

Materials. Chemicals were purchased from commercial sources and used without further purification unless otherwise noted. Decamethylferrocene ($Me_{10}Fc$), octamethylferrocene (Me_8Fc), 1,1′-dimethylferrocene (Me_2Fc), ferrocene (Fc), acethylferrocene (AcFc), 1,1′-dibromoferrocene (Br_2Fc), *N,N,N′,N′*-tetramethylphenylenediamine (TMPD), 2,3,5,6-tetramethylphenylenediamine (2,3,5,6-TMPD), *p*-phenylenediamine (*p*-PDA), and *p*-aminophenol (*p*-AP) were also purchased from commercial sources and used without further purification. Toluene was distilled over sodium-benzophenone ketyl and used for the synthesis of H_2DPP. MeCN (spectrophotometric grade; Nakalai Tesque) was used for spectral measurements. $CHCl_3$ and CH_2Cl_2 used as solvents were distilled over CaH_2 before use. The syntheses of H_2DPP and H_2OPP were performed in accordance with literature procedures.[31] H_2TPP was purchased from a commercial source and used without further purification. $[H_4DPP]Cl_2$ was prepared in accordance with literature methods.[24b] $[H_4TPP]Cl_2$ and $[H_4OPP]Cl_2$ were prepared by adding 3% aqueous HCl (20 mL) to solutions of H_2TPP (200 mg, 0.33 mmol) and H_2OPP (200 mg, 0.22 mmol), respectively, in CH_2Cl_2 (200 mL) in a separating funnels. The organic layers were dried over Na_2SO_4. The solvents were removed using a rotary evaporator, and the products were dried in vacuo at 120 °C. The reaction proceeded quantitatively. $[H_4TMP]Cl_2$ was generated in situ by adding ca. 30 equivs of HCl to a MeCN solution of H_2TMP. The amount of added HCl, which was the minimal amount for stabilization of the hydrochloride salt of H_2TMP, was determined by absorption spectroscopy.

$H_2F_{20}TPP$ was synthesized by the Adler method.[32] To a solution of propionic acid (300 mL) containing 2,3,4,5,6-pentafluorobenzaldehyde (10.1 g, 52 mmol) and acetic anhydride (10.6 g, 104

(16) (a) Gentemann, S.; Medforth, C. J.; Forsyth, T. P.; Nurco, D. J.; Smith, K. M.; Fajer, J.; Holten, D. *J. Am. Chem. Soc.* **1994**, *116*, 7363. (b) Caignan, G. A.; Deshmukh, R.; Zeng, Y.; Wilks, A.; Bunce, R. A.; Rivera, M. *J. Am. Chem. Soc.* **2003**, *125*, 11842. (c) Sigfridsson, E.; Ryde, U. *J. Biol. Inorg. Chem.* **2003**, *8*, 272. (d) Shi, Z.; Franco, R.; Haddad, R.; Shelnutt, J. A.; Ferreira, G. C. *Biochemistry* **2006**, *45*, 2904.

(17) (a) Alden, R. G.; Ondrias, M. R.; Shelnutt, J. A. *J. Am. Chem. Soc.* **1990**, *112*, 691. (b) Cowley, A. B.; Lukat-Rodgers, G. S.; Rodgers, K. R.; Benson, D. R. *Biochemistry* **2004**, *43*, 1656. (c) Cowley, A. B.; Benson, D. R. *Inorg. Chem.* **2007**, *46*, 48. (d) Mbofana, C.; Zimmer, M. *Inorg. Chem.* **2006**, *45*, 2598.

(18) (a) Barkigia, K. M.; Chantranupong, L.; Smith, K. M.; Fajer, J. *J. Am. Chem. Soc.* **1988**, *110*, 7566. (b) Michel, L. V.; Ye, T.; Bowman, S. E. J.; Levin, B. D.; Hahn, M. A.; Russell, B. S.; Elliott, S. J.; Bren, K. L. *Biochemistry* **2007**, *46*, 11753.

(19) (a) Shelnutt, J. A.; Medforth, C. J.; Berber, M. D.; Barkigia, K. M.; Smith, K. M. *J. Am. Chem. Soc.* **1991**, *113*, 4077. (b) Medforth, C. J.; Senge, M. O.; Smith, K. M.; Sparks, L. D.; Shelnutt, J. A. *J. Am. Chem. Soc.* **1992**, *114*, 9859. (c) Nurco, D. J.; Medforth, C. J.; Forsyth, T. P.; Olmstead, M. M.; Smith, K. M. *J. Am. Chem. Soc.* **1996**, *118*, 10918. (d) Nurco, D. J.; Barkigia, K. M.; Renner, M. W.; Melamed, D.; Smith, K.; Fajer, J. *J. Phys. Chem. B* **1998**, *102*, 322.

(20) Takeda, J.; Ohya, T.; Sato, M. *Inorg. Chem.* **1992**, *31*, 2877.

(21) Medforth, C. J.; Hobbs, J. D.; Rodriguez, M. R.; Abraham, R. J.; Smith, K. M.; Shelnutt, J. A. *Inorg. Chem.* **1995**, *34*, 1333.

(22) Shelnutt, J. A.; Majumder, S. A.; Sparks, L. D.; Hobbs, J. D.; Medforth, C. J.; Senge, M. O.; Smith, K. M.; Miura, M.; Luo, L.; Quirke, J. M. E. *J. Raman Spectrosc.* **1992**, *23*, 523.

(23) (a) Medforth, C. J.; Smith, K. M. *Tetrahedron Lett.* **1990**, *31*, 5583. (b) Gentemann, S.; Medforth, C. J.; Forsyth, T. P.; Nurco, D. J.; Smith, K. M.; Fajer, J.; Holten, D *J. Am. Chem. Soc.* **1994**, *116*, 7363. (c) Drain, C. M.; Kirmaier, C.; Medforth, C. J.; Nurco, D. J.; Smith, K. M.; Holten, D. *J. Phys. Chem.* **1996**, *100*, 11984. (d) Gentemann, S.; Nelson, N. Y.; Jaquinod, L.; Nulco, D. J.; Leung, S. H.; Medforth, C. J.; Smith, K. M.; Fajer, J.; Holten, D. *J. Phys. Chem. B* **1997**, *101*, 1247. (e) Retsek, J. L.; Gentemann, S.; Medforth, C. J.; Smith, K. M.; Chirvony, V. S.; Fafer, J.; Holten, D. *J. Phys. Chem. B* **2000**, *104*, 6690. (f) Savenkova, N. S.; Kuznetsova, R. T.; Lapin, I. N.; Svetlichnyi, V. A.; Mayer, G. V.; Shatunov, P. A. *Opt. Spectrosc.* **2005**, *99*, 751.

(24) (a) Harada, R.; Kojima, T. *Chem. Commun.* **2005**, 716. (b) Kojima, T.; Nakanishi, T.; Harada, R.; Ohkubo, K.; Yamauchi, S.; Fukuzumi, S. *Chem.−Eur. J.* **2007**, *11*, 8714. (c) Fukuzumi, S.; Kojima, T. *J. Mater. Chem.* **2008**, *18*, 1427.

(25) Utilization of H_2DPP as a ligand to the Mo(V) center has allowed us to access a "porphyrin nanotube" including unstable and unprecedented tetranuclear Mo(VI)−oxo clusters in its inner space, see:Harada, R.; Matsuda, Y.; Okawa, H.; Kojima, T. *Angew. Chem., Int. Ed.* **2004**, *43*, 1825.

(26) Both protonation of the porphyrin and the substituent groups of the porphyrin play an important role in attaining the ordered assemblies with single-walled carbon nanotubes, see:(a) Hasobe, T.; Fukuzumi, S.; Kamat, P. V. *J. Am. Chem. Soc.* **2005**, *127*, 11884. (b) Hasobe, T.; Fukuzumi, S.; Kamat, P. V. *J. Phys. Chem. B* **2006**, *110*, 25477.

(27) For electron donor−acceptor dyads in which porphyrins are used as electron acceptors, see:(a) Kashiwagi, Y.; Imahori, H.; Araki, Y.; Ito, O.; Yamada, K.; Sakata, Y.; Fukuzumi, S. *J. Phys. Chem. A* **2003**, *107*, 5515. (b) Kubo, M.; Mori, Y.; Otani, M.; Murakami, M.; Ishibashi, Y.; Yasuda, M.; Hosomizu, K.; Miyasaka, H.; Imahori, H.; Nakashima, S. *J. Phys. Chem. A* **2007**, *111*, 5136.

(28) Fukuzumi, S.; Nakanishi, I.; Barbe, J.-M.; Guilard, R.; Van Caemelbecke, E.; Guo, N.; Kadish, K. M. *Angew. Chem., Int. Ed.* **1999**, *38*, 964.

(29) (a) Kadish, K. M.; E, W.; Ou, Z.; Shao, J.; Sintic, P. J.; Ohkubo, K.; Fukuzumi, S.; Crossley, M. J. *Chem. Commun.* **2002**, 356. (b) Ou, Z.; Kadish, K. M.; E, W.; Shao, J.; Sintic, P. J.; Ohkubo, K.; Fukuzumi, S.; Crossley, M. J. *Inorg. Chem.* **2004**, *43*, 2078.

(30) Fukuzumi, S.; Ohkubo, K.; E, W.; Ou, Z.; Shao, J.; Kadish, K. M.; Hutchison, J. A.; Ghiggino, K. P.; Sintic, P. J.; Crossley, M. J. *J. Am. Chem. Soc.* **2003**, *125*, 14984.

(31) (a) Chan, K. S.; Zhou, X.; Luo, B.-S.; Mak, T. C. W. *J. Chem. Soc., Chem. Commun.* **1995**, 733. (b) Liu, C.-J.; Yu, W.-Y.; Peng, S.-M.; Mak, T. C. W.; Che, C.-M. *J. Chem. Soc., Dalton Trans.* **1998**, 1805.

mmol) was added pyrrole (3.6 mL, 54 mmol), and the mixture was refluxed for 3 h. The solvent was distilled off, and the product was purified by silica gel column chromatography using $CHCl_3$ as the eluent. First fraction was collected and dried under reduced pressure. The residue was dissolved in 600 mL of $CHCl_3$/MeOH (1:1 v/v), and $Zn(CH_3COO)_2 \cdot 2H_2O$ (10.0 g, 46 mmol) was added. The mixture solution was refluxed for 3 h and washed with water in a separating funnel, and the organic layers were dried over Na_2SO_4. After the solvent was distilled off the product was purified by silica gel column chromatography using $CHCl_3$ as the eluent. Purple crystals of [Zn(F_{20}TPP)(MeCN)] were obtained from $CHCl_3$/MeCN. Yield: 0.9 g, 8.5%. The crystals were dried in vacuo at 150 °C to remove axial MeCN.

Electrochemical Measurements. Cyclic voltammetry (CV), differential pulse voltammetry (DPV), and second-harmonic ac voltammetry (SHACV)[33,34] were performed on an ALS 630B electrochemical analyzer in deaerated MeCN containing 0.1 M [(*n*-Bu_4)N]PF_6 (TBAPF_6) as a supporting electrolyte at 298 K. A conventional three-electrode cell was used with a platinum working electrode (surface area of 0.3 mm^2) and a platinum wire as the counter electrode. The Pt working electrode (BAS) was routinely polished with BAS polishing alumina suspension and rinsed with acetone before use. The potentials were measured with respect to the Ag/$AgNO_3$ (0.01 M) reference electrode. All potentials (vs Ag/Ag^+) were converted to values vs SCE by adding 0.29 V. All electrochemical measurements were carried out under an atmospheric pressure of argon.[35]

Fluorescence Lifetime Measurements. Fluorescence decays were measured using a Photon Technology International GL-3300 a nitrogen laser with a Photon Technology International GL-302 system equipped with a four-channel digital delay/pulse generator (Standard Research System Inc., model DG535) and a motor driver (Photon Technology International, model MD-5020). The excitation wavelengths were 444 nm with use of POPOP (Exciton Co., Ltd.) and 466 and 488 nm with use of Coumarin 481 (Exciton Co., Ltd.).

Phosphorescence Measurements. An Ar-saturated 2-MeTHF solution containing [H_4DPP]Cl_2, [H_4TPP]Cl_2, and [H_4OPP]Cl_2 at 77 K was excited at each absorption maximum of the Soret band (444 nm for [H_4TPP]Cl_2, 466 nm for [H_4OPP]Cl_2, 488 nm for [H_4DPP]Cl_2) using a Cosmo System LVU-200S spectrometer. Near-IR emission spectra were measured using a SPEX Fluorolog τ3 fluorescence spectrophotometer. A photomultiplier (Hamamatsu Photonics model R5509-72) was used to detect emission in the near-infrared region (band path 2 mm). Phosphorescence of an Ar-saturated 2-MeTHF solution of [H_4TMP]Cl_2 and [Zn(F_{20}TPP)-(MeCN)] in a quartz tube (3 mm in diameter) in liquid nitrogen was measured using a Shimadzu RF-5300PC spectrofluorophotometer by excitation at 440 and 426 nm, respectively.

ESR Measurements. ESR spectra were recorded using a JEOL JES- ME-LX X-band spectrometer at room temperature with photoirradiation (λ > 500 nm) from a USHIO USH1005 D high-pressure mercury arc lamp (1000 W) equipped with a water filter to remove infrared light and a glass cut off filter (Y-49; ASAHI TECHNOGLASS Corp., Japan). The solution was deoxygenated by argon purging for 10 min prior to measurements. The magnitude of modulation was chosen to optimize the resolution and signal-to-noise (S/N) ratio of the observed spectra under nonsaturating microwave power conditions. The *g* value was calibrated using a Mn^{2+} marker.

Theoretical Calculations. Density functional calculations[36] were performed with Gaussian03 (Revision C.02, Gaussian, Inc.)[37] using a spin-restricted B3LYP functional for the closed-shell molecules, [H_4DPP^{2+}]Cl_2, [H_4TPP^{2+}]Cl_2, and [H_4OPP^{2+}]Cl_2, and spin-unrestricted B3LYP functional for the open-shell one-electron reduced species, {[H_4DP$P^{\bullet+}$]Cl_2}$^-$, {[H_4TP$P^{\bullet+}$]Cl_2}$^-$, and {[H_4OP$P^{\bullet+}$]Cl_2}$^-$, on an 8-processor QuantumCube developed by Parallel Quantum Solutions. Since MeCN should be coordinated to [Zn(F_{20}TPP)] as axial ligands in MeCN solution, the structure of [Zn(F_{20}TPP)(MeCN)] is used for DFT calculation. DFT optimizations of [H_4TMP]Cl_2, {[H_4TM$P^{\bullet+}$]Cl_2}$^-$, [Zn(F_{20}TPP)-(MeCN)], and [Zn(F_{20}TPP)(MeCN)]$^{\bullet-}$ were performed on a 32-processor QuantumCube at the B3LYP/3-21G level of theory. Graphical outputs of the computational results were generated with the Gauss View software program (ver. 3.09) developed by Semichem, Inc.[38]

Laser Flash Photolysis Measurements. Measurements of transient absorption spectra were made according to the following procedure: Degassed MeCN solutions containing diprotonated porphyrins and electron donors were excited by a Panther OPO pumped Nd:YAG laser (Continuum, SLII-10, 4−6 ns fwhm) at 444 ([H_4TPP]Cl_2), 466 ([H_4OPP]Cl_2), 488 ([H_4DPP]Cl_2), 440 ([H_4TMP]Cl_2), and 426 nm (Zn(F_{20}TPP)(MeCN)). The resulting time-resolved transient absorption spectra were then measured using a continuous Xe lamp (150 W) and a photodiode (Hamamatsu 2949) as the probe light and detector, respectively. The output from the photodiode and photomultiplier tube was recorded using a digitizing oscilloscope (Tektronix, TDS3032, 300 MHz). The solutions were deoxygenated by argon purging for 10 min prior to measurements. The rates of photoinduced electron-transfer reactions were followed by the decay of the absorption maximum due to the triplet excited state of diprotonated porphyrins under pseudo-first-order conditions. Pseudo-first-order rate constants were determined by a least-squares curve fit using a microcomputer.

Results and Discussion

Photoinduced Electron-Transfer Reduction of Diprotonated Porphyrins. The transient absorption spectrum of [H_4DPP]Cl_2 in acetonitrile (MeCN) exhibited a triplet−triplet absorption band at 550 nm together with bleaching at 490 and 720 nm due to the Soret and Q-band of [H_4DPP]Cl_2 (Figure 1a). The decay of the absorbance at 550 nm due to ^{3}{[H_4DPP]Cl_2}* obeys first-order kinetics, and the rate constant (k_T) of the triplet decay to the ground state is determined to be 4.7×10^4 s^{-1} at 298 K (Figure 1b).

Time-resolved nanosecond transient absorption spectra of [H_4DPP]Cl_2 were measured in the presence of electron donors to examine the dynamics of electron transfer from electron donors to ^{3}{[H_4DPP]Cl_2}* in MeCN at 298 K. Figure 2a shows a typical example of the transient absorption spectral change with use of *N,N,N′,N′*-tetramethylphenylenediamine (TMPD) as an electron donor. The T−T absorption spectrum due to ^{3}{[H_4DPP]Cl_2}* observed at 0.5 μs after laser excitation (○) is changed to the transient absorption spectrum at 10 μs (●) in Figure 2a.

The absorption band at 530 nm was assigned to {[H_4DP$P^{\bullet+}$]Cl_2}$^-$ because the same absorption band was

(32) Adler, A. D.; Longo, F. R.; Finarell, J.; Goldmacher, J.; Assour, J.; Korsakoff, L. *J. Org. Chem.* **1967**, 32.
(33) The SHACV method provides a superior approach to directly evaluate the one-electron redox potentials in the presence of a follow-up chemical reaction relative to the better-known dc and fundamental harmonic ac methods:(a) Bond, A. M.; Smith, D. E. *Anal. Chem.* **1974**, *46*, 1946. (b) Arnett, E. M.; Amarnath, K.; Harvey, N. G.; Cheng, J.-P. *J. Am. Chem. Soc.* **1990**, *112*, 344.
(34) Bard, A. J.; Faulkner, L. R. *Electrochemical Methods, Fundamental and Applications*; John Wiley & Sons: New York, 2001; Chapter 10, pp 368−416.
(35) Mann, C. K.; Barnes, K. K. *Electrochemical Reactions in Non-aqueous Systems*; Mercel Dekker: New York, 1970.
(36) (a) Becke, A. D. *J. Chem. Phys.* **1993**, *98*, 5648. (b) Lee, C; Yang, W.; Parr, R. G. *Phys. Rev. B* **1988**, *37*, 785.
(37) Frisch, M. J.; et al. *Gaussian 03*, Revision C.02; Gaussian, Inc.: Wallingford, CT, 2004. The full list of authors is given in the Supporting Information.
(38) Dennington, R., II; Keith, T.; Millam, J.; Eppinnett, K.; Hovell, W. L.; Gilliland, R. Semichem, Inc.: Shawnee Mission, KS, 2003.

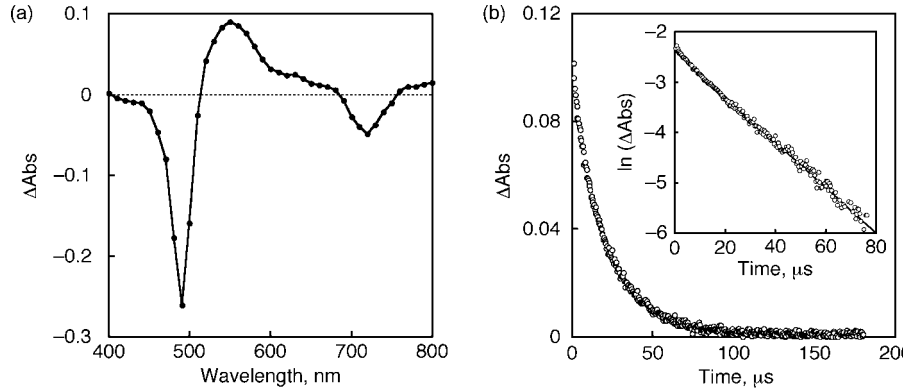

Figure 1. (a) Transient absorption spectrum of $[H_4DPP]Cl_2$ (3.0 μM) in MeCN measured 2 μs after laser excitation at 488 nm. (b) Time profile at 550 nm. (Inset) First-order plot.

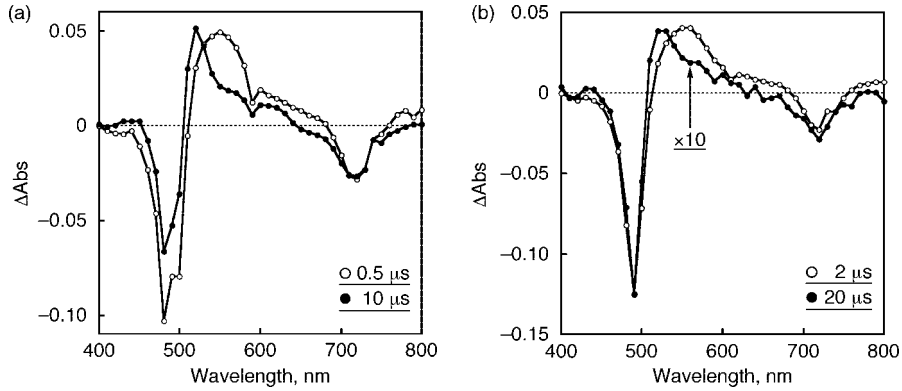

Figure 2. (a) Transient absorption spectra of 3 μM $[H_4DPP]Cl_2$ in the presence of 50 μM TMPD in deaerated MeCN at 298 K taken at 0.5 (○) and 10 μs (●) after nanosecond laser excitation at 488 nm. (b) Transient absorption spectrum of $\{[H_4DPP^{\bullet+}]Cl_2\}^-$ observed in photoinduced electron transfer from 1,1′-dimethylferrocene (50 μM) to $^3\{[H_4DPP]Cl_2\}^*$ in deaerated MeCN at 298 K taken at 2 (○) and 20 μs (●) after nanosecond laser excitation at 488 nm.

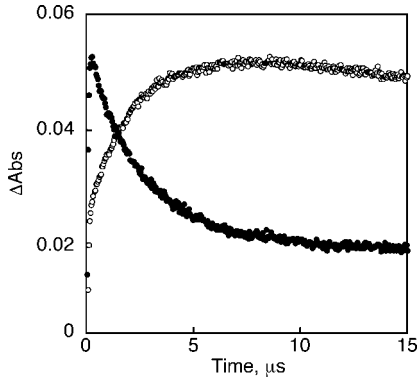

Figure 3. Absorption time profile of 3 μM $[H_4DPP]Cl_2$ in the presence of 50 μM TMPD in MeCN ((○) 520 nm, (●) 550 nm).

observed in the transient absorption spectra in photoinduced electron transfer from 1,1′-dimethylferrocene (Me_2Fc) to $^3\{[H_4DPP]Cl_2\}^*$ as shown in Figure 2b. The same absorption band was observed in the case of other ferrocene and aniline derivatives. The TMPD radical cation ($TMPD^{\bullet+}$) has an absorption maximum at 610 nm ($\epsilon = 1.6 \times 10^4$ M^{-1} cm^{-1}),[39] which is overlapped with the strong T−T absorption of $^3\{[H_4DPP]Cl_2\}^*$. The time profile of the decay of absorbance at 550 nm due to $^3\{[H_4DPP]Cl_2\}^*$ coincides with the rise in the absorbance at 520 nm due to $\{[H_4DPP^{\bullet+}]Cl_2\}^-$, as shown in Figure 3.

Figure 4. ESR spectrum of $TMPD^{\bullet+}$ generated by photoirradiation of an MeCN solution of saturated $[H_4DPP]Cl_2$ and TMPD (0.12 M). Asterisks denote signals of Mn^{2+} markers.

ESR measurements for an MeCN solution of saturated $[H_4DPP]Cl_2$ and TMPD (0.12 M) under photoirradiation ($\lambda >$ 500 nm) afforded an ESR signal with a g value of 2.0031 as shown in Figure 4, which agrees with that of $TMPD^{\bullet+}$ generated thermally using $[Fe(bpy)_3](PF_6)_3$. This value is quite similar to the g value of 2.0028 in 2-propanol and 2.0029 and 2.0033 in the crystal.[40] These results confirm that electron transfer from TMPD to $^3\{[H_4DPP]Cl_2\}^*$ occurs to produce $TMPD^{\bullet+}$ and $\{[H_4DPP^{\bullet+}]Cl_2\}^-$.

The rate of electron transfer obeys pseudo-first-order kinetics as shown in Figure 5a. The pseudo-first-order rate constant increases linearly with the increasing concentration of TMPD as shown in Figure 5b. From the slope of the linear plot depicted in Figure 5b the rate constant of electron transfer from TMPD to $^3\{[H_4DPP]Cl_2\}^*$ is determined to be 4.9×10^9 M^{-1} s^{-1}. A similar spectral change is observed in electron transfer from

(39) Grampp, G.; Neubauer, K. *J. Chem. Soc., Perkin Trans. 2* **1993**, 2015.

(40) (a) Avdievich, N. I.; Jeevarajan, A. S.; Forbes, M. D. E. *J. Phys. Chem.* **1996**, *100*, 5334. (b) Yamauchi, J.; Fujita, H. *Bull. Chem. Soc. Jpn.* **1990**, *63*, 2928.

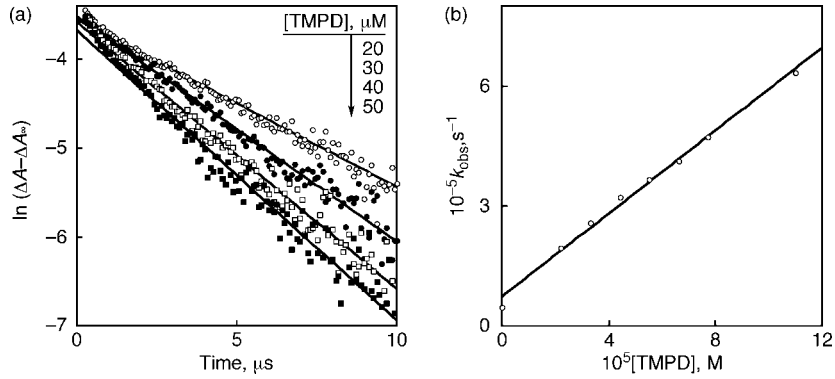

Figure 5. (a) Pseudo-first-order plot of the absorbance of $[H_4DPP]Cl_2$ in the presence of various concentrations ((○) 20, (●) 30, (□) 40, (■) 50 μM) of TMPD in deaerated MeCN at 298 K observed by excitation at 488 nm. (b) Plot of the pseudo-first-order rate constant (k_{obs}) vs the concentration of TMPD.

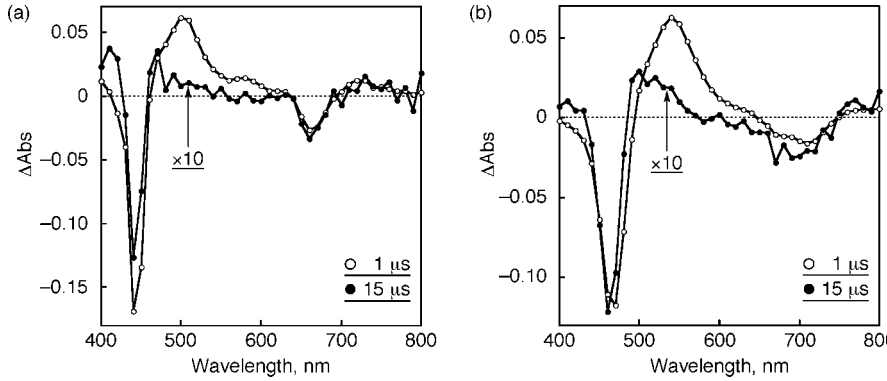

Figure 6. (a) Transient absorption spectra of 3 μM $[H_4TPP]Cl_2$ in the presence of 30 μM Me_2Fc in deaerated MeCN containing 100 μM conc. HCl (35%) at 298 K taken at 1 (○) and 15 μs (●) after nanosecond laser excitation at 444 nm. (b) Transient absorption spectra of 3 μM $[H_4OPP]Cl_2$ in the presence of 50 μM Me_2Fc in deaerated MeCN containing 100 μM conc. HCl (35%) at 298 K taken at 1 (○) and 15 μs (●) after nanosecond laser excitation at 466 nm.

Table 1. One-Electron Oxidation Potentials (E_{ox}) of Electron Donors, Driving Forces of Photoinduced Electron Transfer ($-\Delta G_{et}$) from Electron Donors to $^3\{[H_4DPP]Cl_2\}^*$, $^3\{[H_4OPP]Cl_2\}^*$, $^3\{[H_4TPP]Cl_2\}^*$, $^3\{[H_4TMP]Cl_2\}^*$, and $^3\{[Zn(F_{20}TPP)(MeCN)]\}^*$, and Electron-Transfer Rate Constants (k_{et}) in MeCN at 298 K

		$[H_4DPP]Cl_2$		$[H_4OPP]Cl_2$		$[H_4TPP]Cl_2$		$[H_4TMP]Cl_2$		$[Zn(F_{20}TPP)(MeCN)]$	
donor	E_{ox} vs SCE, V[a]	$-\Delta G_{et}$, eV	k_{et}, M^{-1} s^{-1}	$-\Delta G_{et}$, eV	k_{et}, M^{-1} s^{-1}	$-\Delta G_{et}$, eV	k_{et}, M^{-1} s^{-1}	$-\Delta G_{et}$, eV	k_{et}, M^{-1} s^{-1}	$-\Delta G_{et}$, eV	k_{et}, M^{-1} s^{-1}
$Me_{10}Fc$	−0.13	1.24	1.3×10^{10}	1.31	1.3×10^{10}	1.31	1.5×10^{10}	1.40	1.1×10^{10}	0.80	1.0×10^{10}
Me_8Fc	−0.04	1.15	1.2×10^{10}	1.22	1.4×10^{10}	1.22	1.6×10^{10}	1.31	1.3×10^{10}	0.71	1.1×10^{10}
TMPD	0.12	0.99	4.9×10^9								
2,3,5,6-TMPD	0.15	0.96	4.1×10^9								
Me_2Fc	0.27	0.84	2.8×10^9	0.91	1.1×10^{10}	0.91	1.1×10^{11}	1.00	1.6×10^{10}	0.40	6.1×10^9
p-PDA	0.27	0.84	2.0×10^9								
Fc	0.38	0.73	1.2×10^9	0.80	5.7×10^9	0.80	9.1×10^9	0.89	1.0×10^{10}	0.28	5.2×10^9
p-AP	0.51	0.60	6.9×10^7								
AcFc	0.62	0.49	1.3×10^7	0.56	4.7×10^8	0.56	1.7×10^9	0.65	5.7×10^9		
Br_2Fc	0.69	0.42	4.6×10^6	0.49	1.6×10^8	0.49	7.5×10^8	0.58	3.8×10^8		

[a] Oxidation potentials of electron donors measured in MeCN at 298 K.

Me_2Fc to $^3\{[H_4TPP]Cl_2\}^*$ and Me_2Fc to $^3\{[H_4OPP]Cl_2\}^*$ as shown in Figure 6. The rate constants of electron transfer from Me_2Fc to $^3\{[H_4TPP]Cl_2\}^*$ and $^3\{[H_4OPP]Cl_2\}^*$ are determined to be the same as 1.1×10^{10} M^{-1} s^{-1}, which is significantly larger than the value of $[H_4DPP]Cl_2$ (2.9×10^9 M^{-1} s^{-1}). The difference in the rate constants among $[H_4TPP]Cl_2$, $[H_4OPP]Cl_2$, and $[H_4DPP]Cl_2$ will be discussed later.

The rate constants of electron transfer (k_{et}) from a series of electron transfers to $^3\{[H_4TPP]Cl_2\}^*$, $^3\{[H_4OPP]Cl_2\}^*$, and $^3\{[H_4DPP]Cl_2\}^*$ were determined as in the case of Me_2Fc, and the results are summarized in Table 1 together with the driving force of electron transfer ($-\Delta G_{et}$, in eV). The driving force of electron transfer is determined from the one-electron oxidation potentials of donors (E_{ox}), the one-electron reduction potentials of protonated porphyrins (E_{red}), and the triplet energies ($^3E^*$) using eq 1

$$-\Delta G_{et} = -e(E_{ox} - E_{red}) + {}^3E^* \quad (1)$$

The E_{red} values of $[H_4TPP]Cl_2$ and $[H_4OPP]Cl_2$ in MeCN were determined by CV to be −0.49 and −0.34 V, respectively, and the E_{red} value of $[H_4DPP]Cl_2$ in MeCN was determined by differential pulse voltammogram to be −0.37 V (Figure S1, Supporting Information). The E_{red} values of $[H_4TPP]Cl_2$, $[H_4OPP]Cl_2$, and $[H_4DPP]Cl_2$ in CH_2Cl_2 were also determined by the cyclic voltammograms to be −0.49, −0.38, and −0.46 V (vs SCE), respectively (Figure S2, Supporting Information).

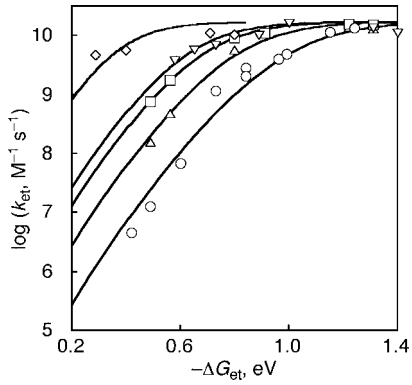

Figure 7. Driving force dependence of log k_{et} for electron transfer from electron donors (Table 1) to ^{3}\{[H_4DPP]Cl_2\}* (○) and ^{3}[Zn(F_{20}TPP)(MeCN)]* (◇) in MeCN at 298 K and ^{3}\{[H_4OPP]Cl_2\}* (△), ^{3}\{[H_4TPP]Cl_2\}* (□), and ^{3}\{[H_4TMP]Cl_2\}* (▽) in MeCN containing ca. 30 equiv of HCl at 298 K, and the fit of the curve based on the Marcus theory of electron transfer (eq 4) is shown by the solid line with λ = 1.69, 1.45, 1.29, 1.21, and 0.84 eV.

Although the E_{red} values of [H_4OPP]Cl_2 and [H_4DPP]Cl_2 are less negative than that of [H_4TPP]Cl_2, the peak separations of the former (190 and 160 mV) are larger than the latter (100 mV) at the same scan rate (100 mV s^{-1}). In each case, the peak separation increases with increasing scan rate. These results indicate that the electron-transfer reduction of [H_4OPP]Cl_2 and [H_4DPP]Cl_2 is thermodynamically more favorable but that the intrinsic barrier of electron transfer is higher as compared with [H_4TPP]Cl_2.

From the absorption and emission maxima the energy of the singlet excited state of [H_4DPP]Cl_2 is determined to be 1.72 eV and the fluorescence lifetime of [H_4DPP]Cl_2 in MeCN was determined to be 1.4 ns. The fluorescence lifetimes of [H_4TPP]Cl_2 and [H_4OPP]Cl_2 in MeCN were also determined to be 3.4 and 1.2 ns. These lifetimes are too short to examine intermolecular photoinduced electron transfer from electron donors to the singlet excited states of the hydrochloride salt of those porphyrins (Figure S3, Supporting Information). This is the reason why we examined photoinduced electron-transfer reactions of the triplet excited states, ^{3}\{[H_4TPP]Cl_2\}*, ^{3}\{[H_4OPP]Cl_2\}*, and ^{3}\{[H_4DPP]Cl_2\}* with electron donors. The triplet excited energies (^3E*) of ^{3}\{[H_4TPP]Cl_2\}*, ^{3}\{[H_4OPP]Cl_2\}*, and ^{3}\{[H_4DPP]Cl_2\}* were determined from the phosphorescence (744, 818, and 838 nm) to be 1.67, 1.52, and 1.48 eV, respectively (Figure S4, Supporting Information).

The driving-force dependence of log k_{et} for electron transfer from a series of electron donors to ^{3}\{[H_4DPP]Cl_2\}* is shown in Figure 7. According to a general scheme of intermolecular photoinduced electron transfer,[41] electron transfer from an electron donor (D) to ^{3}\{[H_4DPP]Cl_2\}* may occur as shown in Scheme 1, where k_{12} and k_{21} are the diffusion rate constant and dissociation rate constant in the encounter complex and k_{ET} is the first-order rate constant of electron transfer in the encounter complex.[42] The observed second-order rate constant of electron transfer (k_{et}) is given by eq 2

$$k_{et} = k_{ET}k_{12}/(k_{21} + k_{ET}) \quad (2)$$

The dependence of k_{ET} on the driving force of electron transfer ($-\Delta G_{et}$) for adiabatic outer-sphere electron transfer has well been established by Marcus as given by eq 3

$$k_{ET} = (k_BT/h)\exp[-(\lambda/4)(1 + \Delta G_{et}/\lambda)^2/k_BT] \quad (3)$$

where k_B is the Boltzmann constant, h is the Planck constant, and λ is the reorganization energy of electron transfer.[13,43] From eqs 2 and 3 is derived eq 4

$$k_{et} = k_{12}Z\exp[-(\lambda/4)(1 + \Delta G_{et}/\lambda)^2/k_BT]/(k_{12} + Z\exp[-(\lambda/4)(1 + \Delta G_{et}/\lambda)^2/k_BT] \quad (4)$$

where Z [= $(k_BT/h)(k_{12}/k_{21})$] is the collision frequency that is taken as 1×10^{11} M^{-1} s^{-1}. The k_{12} value is the diffusion rate constant in MeCN that is taken as 2.0×10^{10} M^{-1} s^{-1}.

The driving-force dependence of the log k_{et} values of photoinduced electron transfer from electron donors to ^{3}\{[H_4DPP]Cl_2\}* is best fitted by the solid line in Figure 7 with a λ value of 1.69 eV. The driving-force dependence of the log k_{et} values in the case of ^{3}\{[H_4TPP]Cl_2\}* and ^{3}\{[H_4OPP]Cl_2\}* is also shown in Figure 7, and this is fitted by the solid line with λ values of 1.29 and 1.45 eV, respectively. In this case, a minimal amount of HCl (ca. 30 equiv) was required to keep formation of [H_4TPP]Cl_2 and [H_4OPP]Cl_2. On the other hand, there was no need to add HCl to [H_4DPP]Cl_2 in MeCN. This indicates that the basicity of H_2DPP, which is the conjugated base of H_4DPP^{2+}, is much larger than that of water. Under acidic conditions, the number of electron donors that can be used in the photoinduced electron-transfer reactions is limited as compared with the case of [H_4DPP]Cl_2 because aniline derivatives, such as TMPD, 2,3,5,6-TMPD, *p*-PDA, and *p*-AP in Table 1, are protonated to lose the electron-donating ability. The reorganization energy of [H_4TMP]Cl_2, which is less distorted than [H_4TPP]Cl_2, is determined to be 1.21 eV. The reorganization energy of [Zn(F_{20}TPP)(MeCN)], which is a planar porphyrin used for comparing the effect of distortion on λ and is relatively easy to reduce, is also determined to be 0.84 eV. The results of transient absorption spectral measurements, cyclic voltammetry, and phosphorescence spectroscopy for [H_4TMP]Cl_2 and [Zn(F_{20}TPP)(MeCN)] are given in Figure S5−S10 and and Table S1, Supporting Information.

Since diprotonated porphyrin dications are known to exhibit saddle distortion due to the steric repulsion of N−H protons,[24b,44]

Scheme 1

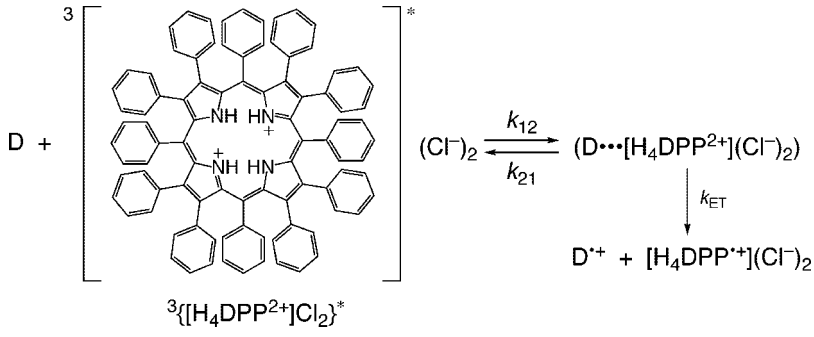

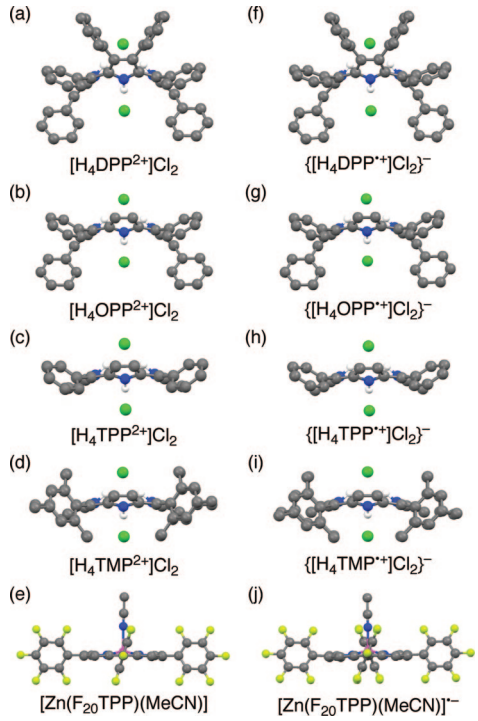

Figure 8. Optimized structures of (a) $[H_4DPP^{2+}]Cl_2$, (b) $[H_4OPP^{2+}]Cl_2$, (c) $[H_4TPP^{2+}]Cl_2$, (d) $[H_4TMP^{2+}]Cl_2$, (e) $[Zn(F_{20}TPP)(MeCN)]$, (f) $\{[H_4DPP^{\bullet+}]Cl_2\}^-$, (g) $\{[H_4OPP^{\bullet+}]Cl_2\}^-$, (h) $\{[H_4TPP^{\bullet+}]Cl_2\}^-$, (i) $\{[H_4TMP^{\bullet+}]Cl_2\}^-$, and (j) $[Zn(F_{20}TPP)(MeCN)]^{\bullet-}$ obtained by DFT calculations at the B3LYP/3-21G level of theory. Hydrogen atoms of the phenyl groups are omitted for clarity.

it is reasonable that the optimized structures of $[H_4DPP]Cl_2$, $[H_4OPP]Cl_2$, $[H_4TPP]Cl_2$, and $[H_4TMP]Cl_2$ are in saddle-distorted structures as shown in Figure 8. In contrast to diprotonated porphyrin dications, $[Zn(F_{20}TPP)(MeCN)]$ is known to be planar.[45] The optimized structures of $[Zn(F_{20}TPP)(MeCN)]$ and one-electron reduced species of $[H_4DPP]Cl_2$, $[H_4OPP]Cl_2$, $[H_4TPP]Cl_2$, $[H_4TMP]Cl_2$, and $[Zn(F_{20}TPP)(MeCN)]$ are also shown in Figure 8. The chloride ions are hydrogen bonded to the N−H protons that are directed to the upper and lower sides of the mean porphyrin plane in the diprotonated species. The hydrogen bonding between the positively charged $N-H^+$ of pyrroles and the chloride anions should be weakened by the electron-transfer reduction of the porphyrin and the calculated hydrogen-bond lengths in the one-electron reduced species presented in Table 2 strongly support the assumption. The difference in the interatomic distances between pyrrole nitrogen atoms and chloride ions in hydrogen bonding ($N-H\cdots Cl^-$) before and after electron transfer was enlarged in accordance with an increase in the number of peripheral phenyl groups.

Table 2. Interatomic Distances $N\cdots Cl^-$ and $Cl^-\cdots Cl^-$ of $[H_4DPP]Cl_2$, $[H_4OPP]Cl_2$, $[H_4TPP]Cl_2$, and $[H_4TMP]Cl_2$ Before and After Electron Transfer Based on DFT Calculations at the B3LYP/3-21G Level of Theory

entry	N(−H)···Cl⁻ (Å)	ΔN(−H)···Cl⁻ (Å)	Cl⁻···Cl⁻ (Å)	Δ Cl⁻···Cl⁻ (Å)
$[H_4DPP^{2+}]Cl_2$	3.22	0.07, 0.08	5.02	0.17
$\{[H_4DPP^{\bullet+}]Cl_2\}^-$	3.29, 3.30		5.19	
$[H_4OPP^{2+}]Cl_2$	3.13, 3.17	0.05, 0.07	4.87	0.16
$\{[H_4OPP^{\bullet+}]Cl_2\}^-$	3.18, 3.24		5.03	
$[H_4TPP^{2+}]Cl_2$	3.10	0.05, 0.06	4.77	0.15
$\{[H_4TPP^{\bullet+}]Cl_2\}^-$	3.15, 3.16		4.92	
$[H_4TMP^{2+}]Cl_2$	3.11	0.05, 0.06	4.80	0.17
$\{[H_4TMP^{\bullet+}]Cl_2\}$	3.16, 3.17		4.97	

Table 3. Root-Mean-Square out-of-Plane Displacement (Δrms) and Reorganization Energy of Porphyrin Dications and $[Zn(F_{20}TPP)(MeCN)]$

entry	Δrms, Å[a]	λ, eV
$[H_4DPP^{2+}]Cl_2$	0.81 (0.82)[b]	1.69
$\{[H_4DPP^{\bullet+}]Cl_2\}^-$	0.84	
$[H_4OPP^{2+}]Cl_2$	0.65	1.45
$\{[H_4OPP^{\bullet+}]Cl_2\}^-$	0.67	
$[H_4TPP^{2+}]Cl_2$	0.46 (0.46)[c]	1.29
$\{[H_4TPP^{\bullet+}]Cl_2\}^-$	0.49	
$[H_4TMP^{2+}]Cl_2$	0.39	1.21
$\{[H_4TMP^{\bullet+}]Cl_2\}^-$	0.38	
$[Zn(F_{20}TPP)(MeCN)]$	0.05 (0.02)[d]	0.84
$[Zn(F_{20}TPP)(MeCN)]^{\bullet-}$	0.05	

[a] Δrms values determined from the crystal structure for porphyrin dication moieties are given in parentheses. [b] Calculated using crystallographic data reported in ref 24a. [c] Calculated using crystallographic data reported in ref 44e. [d] Calculated using crystallographic data reported in ref 45.

In order to clarify the degree of the distortion in the doubly protonated porphyrins we adopted root-mean-square out-of-plane displacement (Δrms), which is defined as eq 5[46]

$$\Delta\text{rms} = \sqrt{\frac{1}{24}\sum_{i=1}^{24}\delta_i^2} \qquad (5)$$

where δ_i is the orthogonal displacement of atom i in the macrocycle from the mean plane. The sum includes all 24 atoms of the porphyrin macrocycle. The Δrms values of $[H_4TMP]Cl_2$, $[H_4TPP]Cl_2$, $[H_4OPP]Cl_2$, $[H_4DPP]Cl_2$, and $[Zn(F_{20}TPP)(MeCN)]$ and reorganization energies (λ) in their photoinduced electron-transfer reduction are summarized in Table 3. The Δrms values determined from the crystal structure for porphyrin dication moieties are given in parentheses, which agree well with those obtained by DFT calculations.

The reorganization energy consists of the solvent reorganization energy (λ_s) and intramolecular reorganization energy (λ_i), that is, $\lambda = \lambda_s + \lambda_i$.[13] The reorganization energies for the electron-transfer reduction of saddle-distorted porphyrin dications are larger than that reported for the electron-transfer oxidation of mesoporphyrin-IX dimethyl ester in MeCN (1.04 eV), which is assumed to be mainly derived from the solvent reorganization energy (λ_s).[47] The λ values for the electron-transfer reduction of saddle-distorted porphyrin dications are also large as compared with the reorganization energy for the electron-transfer reduction of planar $[Zn(F_{20}TPP)(MeCN)]$. This shows that the λ values of saddle-distorted porphyrin dications

(41) (a) Rehm, D.; Weller, A. *Ber. Bunsen-ges Phys. Chem.* **1969**, *73*, 834. (b) Rehm, D.; Weller, A. *Isr. J. Chem.* **1970**, *8*, 259.
(42) Kavarnos, G. J. *Fundamentals of Photoinduced Electron Transfer*; Wiley−VCH: New York, 1993.
(43) Brunschwig, B. S.; Ehrenson, S.; Sutin, N. J. *J. Am. Chem. Soc.* **1984**, *106*, 6858.
(44) Crystal structures of tetraphenylporphyrin diacids:(a) Stone, A.; Fleischer, B. *J. Am. Chem. Soc.* **1968**, *90*, 2735. (b) Fleischer, E. B. *Acc. Chem. Res.* **1970**, *3*, 105. (c) Cheng, B.; Munro, O. Q.; Marques, H. M.; Scheidt, W. R. *J. Am. Chem. Soc.* **1997**, *119*, 10732. (d) Juillard, S.; Ferrand, Y.; Simonneaux, G.; Toupet, L. *Tetrahedron* **2005**, *61*, 3489. (e) Rayati, S.; Zakavi, S.; Ghaemi, A.; Carroll, P. J. *Tetrahedron Lett.* **2008**, *49*, 664.
(45) Birnbaum, E. R.; Hodge, J. A.; Grinstaff, M. W.; Schaefer, W. P.; Henling, L.; Labinger, J. A.; Bercaw, J. E.; Gray, H. B. *Inorg. Chem.* **1995**, *34*, 3625–3632.
(46) Jentzen, W.; Turowska-Tyrk, I.; Scheidt, W. R.; Shelnutt, J. A. *Inorg. Chem.* **1996**, *35*, 3559.
(47) Marguet, S.; Hapiot, P.; Neta, P. *J. Phys. Chem.* **1994**, *98*, 7136.

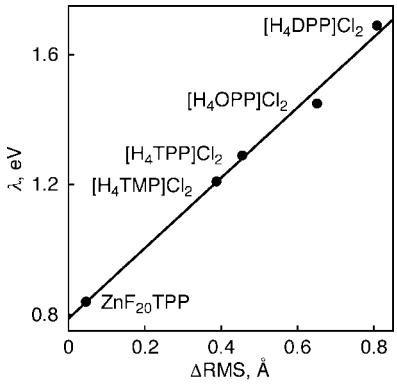

Figure 9. Relationship between λ values in the photoinduced electron-transfer reduction of diprotonated porphyrin dications in MeCN and root-mean-square out-of-plane displacements (Δrms).

largely depend on not only λ_s but also the intramolecular reorganization energy (λ_i), which is mainly due to the resultant structural change of the entity. The contribution of λ_i becomes larger in accordance with an increase of the degree of displacements of atoms, and the increase of λ is positively correlated with the Δrms value of the hydrochloride salt of porphyrins and [Zn(F_{20}TPP)(MeCN)] as depicted in Figure 9.

Since the solvent term of the reorganization energy can be assumed to be the same, the linear correlation between the reorganization energy and the distortion of the porphyrin ring (Δrms) clearly indicates that the distortion governs the intramolecular term of the reorganization energy and the larger distortion gives rise to the larger λ_i. The differences in Δrms values of porphyrin dications before and after electron transfer are approximately the same; however, the difference in the distance of hydrogen bonding among the pyrrole N−H protons and the chloride anions (N−H···Cl^-) become larger with increasing Δrms values (Table 2). This indicates that the elongation of the hydrogen bond is the main factor for the increase of λ_i. This observation is similar to that in the oxidation of metalloporphyrins, which exhibit large reorganization energies due to the large changes in coordination bond lengths around metal centers before and after electron transfer.[1,14] Such correlation between the molecular distortion and reorganization energy was observed in the type 1 copper site of M98Q amicyanin.[48] Thus, we can conclude that the change in λ_i is originated from that in the hydrogen bonding among pyrrole N−H protons and chloride anions, that is, weakening of hydrogen bonding. This weakening of hydrogen bonding gives rise to the larger distortion as represented by the larger Δrms in the one-electron reduced species (Table 2) to exemplify the larger λ_i values.

(48) Ma, J. K.; Mathews, S.; Davidson, V. L. *Biochemistry* **2007**, *46*, 8561.

Concluding Remarks

Doubly protonated porphyrin dications showing saddle-distorted structures due to the steric effect of pyrrole N−H protons can act as electron acceptors due to the elevated reduction potentials which are comparable to those of fullerenes and quinones. Photoexcitaion of those porphyrin dications gives rise to the triplet excited state that undergoes photoinduced electron transfer to afford the one-electron reduced π-radical cations of diprotonated porphyrins and radical cations of electron donors. Among such distorted porphyrins, H_2DPP with intrinsic saddle distortion originating from the steric hindrance among peripheral phenyl groups can form stable diprotonated species in sharp contrast to H_2TPP and H_2OPP that can afford such species only under strongly acidic conditions. In the photoinduced electron transfer the reorganization energy of the porphyrin dication has been revealed to be regulated by the intramolecular reorganization energy that is governed by the large structural change of the distorted porphyrin in the course of electron transfer. This is supported by the linear relationship between the out-of-plane displacements and the reorganization energies of electron transfer as represented in Figure 9. The clarification of such electron-transfer properties of nonplanar diprotonated porphyrins provides invaluable information to establish a new aspect of porphyrins and utilize their novel functions based on the saddle distortion of the porphyrin core.

Acknowledgment. The support of a Grant-in-Aid (Nos. 18033033, 19205019, and 19750034) and a Global COE program, "the Global Education and Research Center for Bio-Environmental Chemistry", from the Ministry of Education, Culture, Sports, Science and Technology, Japan, is gratefully acknowledged. We also appreciate support from the Japan Science and Technology Agency (JST) through the "Potentiality verification stage" program.

Supporting Information Available: CV and DPV traces, plots of fluorescence decay, phosphorescence spectra for [H_4TPP]Cl_2, [H_4OPP]Cl_2, and [H_4DPP]Cl_2; transient absorption spectra, CV, and phosphorescence spectrum of [H_4TMP]Cl_2 and [Zn(F_{20}TPP)-(MeCN)]; full author list of ref 37. This material is available free of charge via the Internet at http://pubs.acs.org.

JA806261Q